International Journal of Nanoelectronics and Materials
Volume 15 (Special Issue) December 2022 [165-181]

Review of Recent Optical Bio-Sensor Based FBG

Deyhaa A. Resen[1,2], Mohammed F. Mohammed[1], and Makram A. Fakhri[3,*]

[1]Al-Nahrain University, College of Engineering, Laser and Optoelectronics Engineering, Iraq
[2]Middle Technical University, Institute of Technology, Baghdad, Iraq
[3]Laser and Optoelectronic Engineering Department, University of Technology-Iraq, Baghdad, Iraq

ABSTRACT

Optical biosensors based on Fiber Bragg Grating (FBG) have been widely used and studied recently due to their considerable advantages. There are many applications in which different types of optical FBG are used as biosensors depending on the different modifications. The FBG is basically a temperature or strain sensor, however, it can be used for more complex applications by modifying and controlling its main parameters such as the periods, refractive index (RI), or adding a sensitive material externally to induce a wavelength shift in the Bragg wavelength λB, phase shift, power variation which can be utilized as a parameter transducer. Therefore, the FBG can be used to measure strain, force, temperature, pressure, vibration, displacement, bio-sensor, etc. In this paper, the state of the optical biosensor based on FBGs sensors, including recent bio-sensors based on tilted FBG, Uniform FBG, Chirped FBG, Long period grating, Phase-Shifted FBG, and photonics crystal fiber (PCF) FBG, have been presented. The principles of work of each kind of FBG biosensor are concisely described.

Keywords: Bio-sensors based on tilted FBG, Uniform FBG, Chirped FBG, Long period grating, Phase-Shifted FBG, photonics crystal FBG

1. INTRODUCTION

FBG is among the most popular optical sensors due to its distinctive qualities such as simple manufacture and highly efficient reflected wavelength [1-3]. FBGs are written as periodic changes in the index of the refraction (RI) through the core over the longitudinal direction [4-6]. It can be formed by different techniques [7-9]. FBGs have potential applications for many optical sensing purposes [10-12]. The optical path difference due to RI change and/or geometry change is the principle of work of FBGs sensors [13-15]. More complex sensing tasks can be achieved utilizing internal or external modification over the FBGs region like temperature [16-18], strain [19-21], stress [22-24], pressure [25-27], bending [28-30], and biological sensors [31-33]. There are different types of FBGs employed in biological applications [34-38]. These applications depend on the FBGs structures and its main operator [39, 40], and the ambience on the other hand, such as Uniform FBG [41, 42], Long period grating [43, 44], Chirped FBG, tilted FBG [45, 46], Phase-Shifted FBG [47, 48], and photonics crystal FBG [49, 50]. This article presents a review of recently used types of biological sensors based on FBGs as seen in Figure 1.

* Makram.A.Fakhri@uotechnology.edu.iq

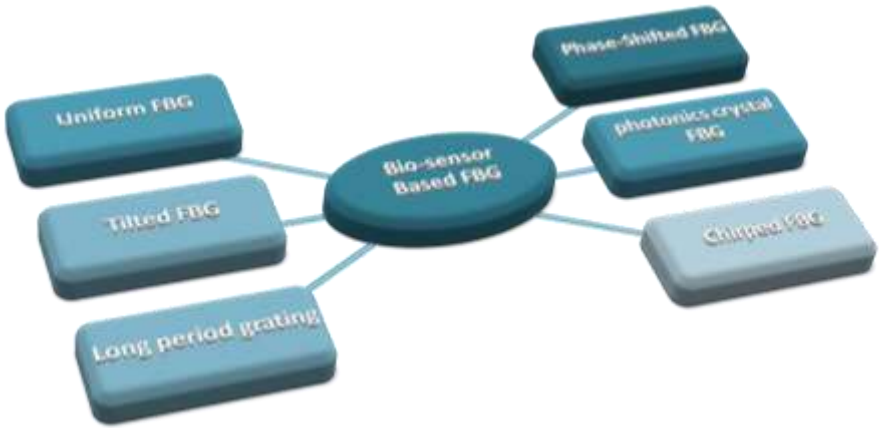

Figure 1. Flowchart of the reviewed FBG sensors.

2. LITERATURE AND THE STATE-OF-THE-ART

2.1 Uniform FBG

Kavitha B. S et al [51] looked into the creation of a label-free, extremely sensitive DNA detection method. This study suggests an etched Fiber Bragg Grating (eFBG) sensor with reduced graphene oxide (rGO) coating can be used to detect and quantify dsDNA. The limit of detection of this proposal is about 261.87 pg/µl and it has a linear response to the concentration of dsDNA through the range from (1 to 50) ng/µl, the repeatability and stability of this work are excellent in this case. Furthermore, the proposal proposes a method for quantifying the amount of DNA attached to the sensor, and thus, UV spectroscopy was used to determine the rGO coating's DNA binding efficacy on the sensor. Figure 2 represents the etched Fiber Bragg Grating (eFBG).

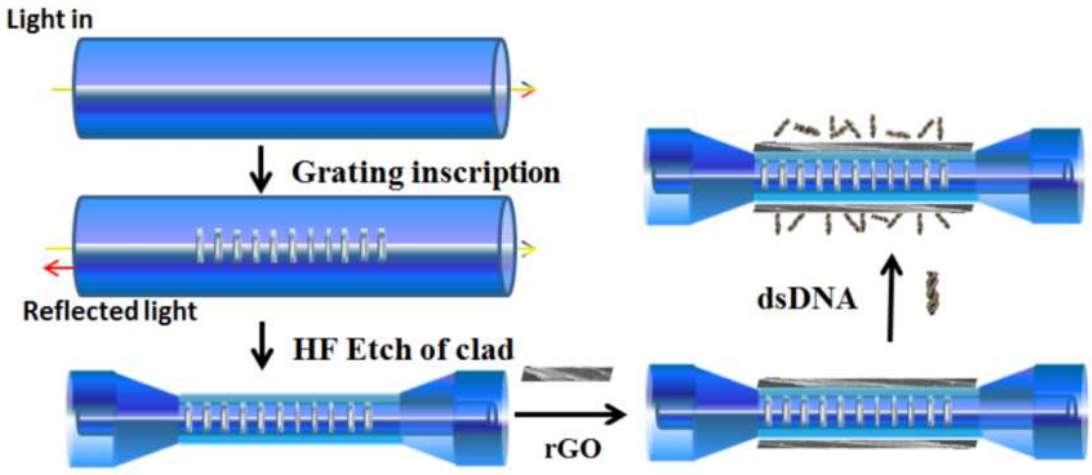

Figure 2. The procedures of eFBG manufacturing and attaching DNA to the sensor. The eFBG sensor's rGO coating pulls dsDNA in.

The FBG in this work is made utilizing the phase mask technique over an SMF doped with germanium has an absorption region of 248nm. The phase mask periodicity is proportional to the λB of FBG. The core and cladding diameters of the used fiber are 9µm and 125µm respectively. The FBG clad is partially removed near the region of the grating using a 50µl, 40% HF bath for 90 minutes. The diameter of the cladding reduced from 125µm to 10µm during etching. The spectrum of λB before and after etching is shown in Figure 3.

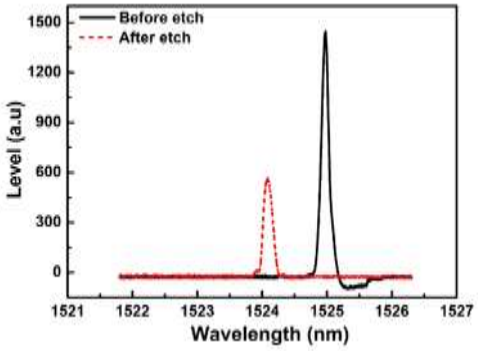

Figure 3. The λ_B spectrum with and without etching.

The hydrophobic is used as clad material. To allow for further molecule attachment, it must be made hydrophilic. This is accomplished by immersing the FBG in a 1:1:5 solution of NH4OH: H2O2: H2O to use OH groups to functionalize the surface of eFBG. The eFBG is subsequently coated with reduced rGO that boosts the ratio of surface-to-volume and makes it easier to attach. The green synthesis process, which utilizes ascorbic acid as the reducing agent, is used to make the rGO. The sensor is immersed in 50µl of rGO until it dries entirely. At room temperature, it needs around 4 hours to be dried. Figure 4 shows: (A) the sensitivity response of the proposed eFBG which is (7.38 nm/RIU) and (1.59 nm/RIU) without and with coating respectively, B) the wavelength shift of a single FBG sensor through 5 stages: a&b) without and with etching respectively, C) with rGO coating, D) prior to the incubation of dsDNA (after immersing in Tris buffer), and e) after incubation with 1.52 µM dsDNA. C) The response of the temperature sensor over time. D) The wavelength shift of FBG, $\Delta\lambda B = \lambda B$ (before and after DNA incubation), as a linear dsDNA concentration function with an error bar (n=3) [52, 53].

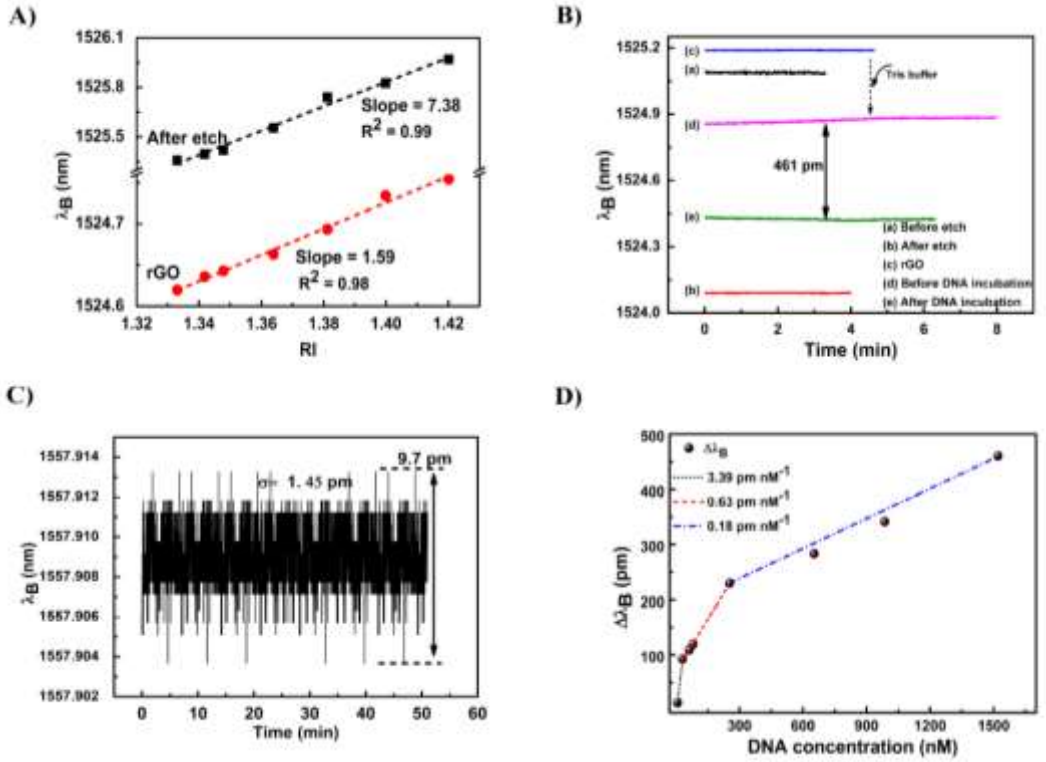

Figure 4. A) Sensitivity of the proposed eFBG sensor. B) The shifting in λB through the 5 stages. C) The response of FBG to the temperature over time. D) The shifting of FBG, $\Delta\lambda B = \lambda B$ (prior to and following DNA insertion), as a linear dsDNA concentration function with an error bar (n=3).

Figure 5 shows the response of wavelength to the amount of concentration of DNA that is attached to the surface of the sensor in (ng).

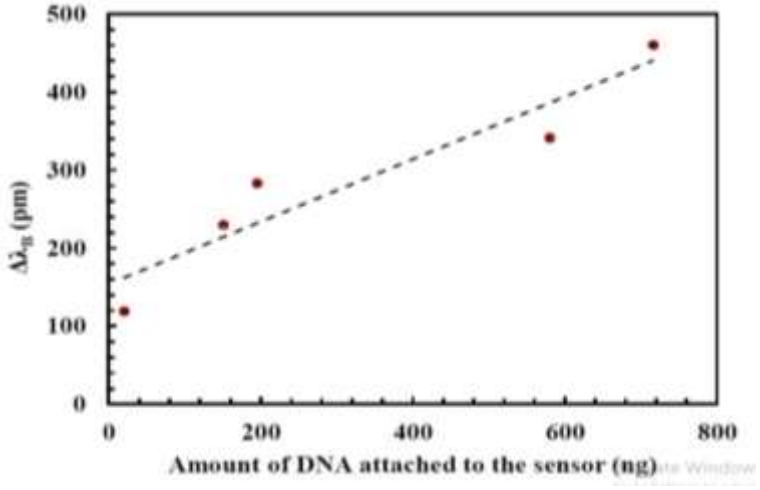

Figure 5. λ_B vs the sensor's DNA attachment density (ng).

The construction of an eFBG sensor functionalized with thinned rGO for dsDNA detection is described in this study. The new eFBG sensor allows for label-free, real-time detection of DNA. The sensitivity of eFBG sensor coated with rGO is high, with a detection limit of 261.87 pg/µl of dsDNA, making it higher in sensitivity in comparison with the commonly used UV spectrometry quantification technique. In concentration of the dsDNA ranged from 1 ng/µl to 50 ng/µl, the sensor likewise demonstrates a linear response. Fluorescence microscopy confirms the dsDNA's binding to the fiber. The rGO-coated eFBG is a dependable DNA sensing platform because of its high stability and reproducibility using UV spectroscopy, the research investigates the response of eFBG and DNA amount bonded to the rGO. This research examines the rGO coating effectiveness on the sensor in terms of DNA attachment and proposes a way for comparing the performance of different types of functionalization procedures on eFBG sensors. The ability to quantify the performance of a functionalization technique could bring the development of extremely sensitive FBG sensors with a wider dynamic range [54, 55].

2.2 Long Period Grating Biosensor (LPG)

Flavio Esposito et al. [56] present a LPG as a biosensor. An LPG is an FBG that is a few centimeters long and has a periodic disruption in the range of 100 to 1000 µm. The LPG induces the coupling between the core and cladding. Consequently, discrete attenuation bands can be seen in the transmitted spectrum of the sensor at wavelengths λres, i that satisfy the phase-matching criterion, the λres, i is given by [57]:

$$\lambda_{res,i} = (n_{eff,co} - n_{eff,cl}).\Lambda \quad (1)$$

Where $n_{eff,co}$ and $n_{eff,cl}$ represent the core mode effective refractive index and the i-th mode of the clad, respectively, Λ represents the period of LPG. Because of its intrinsic sensitivity to the outer index of the cladding modes, the LPG is very interested in biological sensing. The RI change generated by the effect of a biological receptor transplanted onto the surface of FBG region on the analyte is the basis for this type of work [58]. Because the mode transition induces high SRI sensitivity, which achieves very low detection limits, the high RI deposition onto the surface of LPG is necessary. Figure 6 depicts the suggested optical transducer, which is made up of a W-type RI profile LPG with DCF and a nanometric layer of graphene oxide.

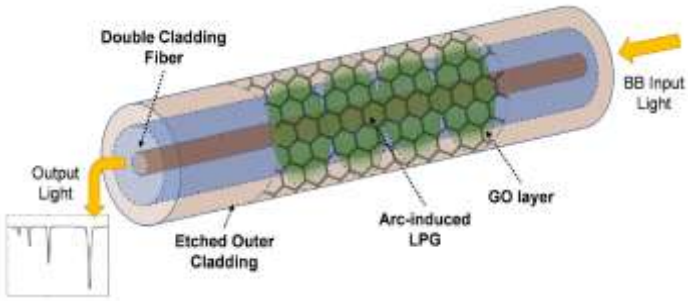

Figure 6. Schematic diagram of LPG in DCF coated with GO.

The W-shaped RI provides a higher RI in the outer cladding than the inner cladding; therefore, some modes can propagate through the outer cladding without interaction with the modes of the core. However, Transition modes from outer to inner cladding can be generated by chemical etching, resulting in a significant increase in SRI sensitivity. The LPG is then coated utilizing a GO thin layer for presenting an interaction between the receptors and analyte on the surface of the sensor [59].

Antibody/antigen interactions can now be accurately detected by employing a novel approach. Furthermore, because of the groups of carboxylic, the nanometric coating deposition of graphene oxide gives ability for direct functionalization of the fiber surface. The bands of attenuation which is compatible with the 5th and 6th order modes of cladding can be seen at 1232 nm and 1377 nm, respectively, in Figure 7, which displays the relationship between transition in [dB] and wavelength [60, 61].

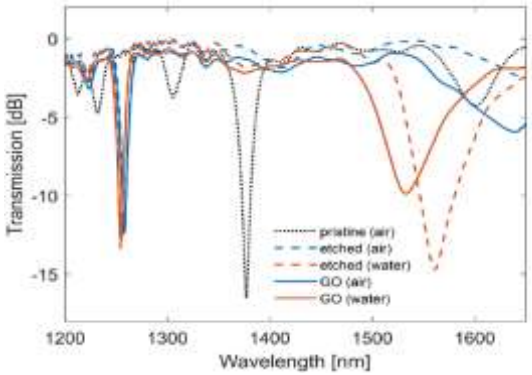

Figure 7. LPG Spectra in a double-cladding fiber (it's known as LPG-B): black dotted is after design, blue dashed is after etching in air and orange dashed is after etching in water, and blue is after GO deposition in air and orange dashed is deposition in water.

In conclusion, in this paper, a fiber-optic-based label-free biosensor is investigated for the development and testing of a new technique. The performance was verified by the C-reactive protein (CRP) detection in serum. The sensor is constructed based on an LPG in a double-cladding fiber utilizing a W-shaped refractive index (RI) profile. As a result, the mode transition inside an all-silica structure achieves a large increase in sensitivity and great visibility of the grating resonances. The LPG was coated with a thin layer of graphene oxide nanometric to give functional groups for the biological recognition element's covalent immobilization [62]. Liang Liu et al. [63] reported two LPG-based biosensors for the detection of streptavidin (SV) and immunoglobulin M (IgM). Three layers of Poly (allylamine hydrochloride)/gold-coated silica nanoparticles are applied to the LPG. The SV concentration in water used for detection ranged from 1.25 nM to 2.7 M, for SV detection, and the LPG sensor has a high sensitivity of 3.88 (ng/ mm2)-1 and a detection limit of 0.86 pg/mm2. The detection threshold is 22 times lower than in earlier research.

C. Liu et al. [64] presented graphene oxide (GO) nanosheet (LPG) hemoglobin sensing with the ultrasensitive sensor. The sensitivity of RI of GO-LPG was around -76.5 dB/RIU, -234.2 dB/RIU, and +1580.5 dB/RIU for RI regions of 1.33-1.38, 1.40-1.44, and 1.45-1.46, respectively, in this work with substantially thicker GO covering. With a sensitivity of roughly 1.9 dB/(mg/mL) and a detectable concentration of 0.05 mg/mL, the GO-LPG was utilized as a biosensor to detect human hemoglobin, which was well below the hemoglobin threshold value for anemia specified by the World Health Organization.

Flavio Esposito et al. [65] presented a single-ended ultrasensitive biosensor (LPG). The LPG was coated with a multilayer system made up of a polycarbonate (PC) film and a thin layer of graphene oxide (GO). The highly stable streptavidin-biotin binding was used to assess the LPG performance level. The observed concentrations range from 0.1 to 1000 aM, with a detection limit of less than 0.2 aM, one of the lowest ever achieved with this sensing technique. Mandeep Singh and Sanjeev Kumar Raghuwanshi [66] developed a TiO_2-coated etched (LPG) biosensor which used to detect Escherichia coli bacteria in food items. The used detection range is 0 cfu/ml–50 cfu/ml. The 40 nm TiO_2 thin film has been used in over LPG in this case. The sensitivity of this work is 2.55 nm/RIU.

2.3 Chirped Fiber Bragg Grating Sensors (CFBG)

This work proposes the use of a shallow-tapered CFBG with a diameter of taper waist of about 39 μm [67]. The proposed structure is shown in Fig (8). The change in intensity occurs when the RI is changed. The shifting in wavelength of the whole spectrum will be detected. As a result, the new structure ensures that each temperature is measured separately. A sample with a CFBG taper waist of 39 m is described here, allowing dual RI–temperature detection [68].

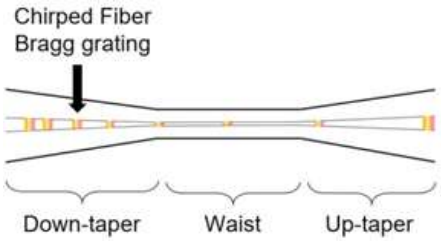

Figure 8. Shallow-tapered (CFBG).

This paper describes a gold-coated shallow-tapered chirped fiber Bragg grating (stCFBG) for both temperature and RI monitoring. The length of the proposed FBG is 15-mm, by tapering a 7.29-mm region with a waist of 39 μm. in this device there are two regions, thepre-taper region, and the post-taper region. The pre-taper region is RI-independent in the stCFBG and it can detect the temperature variation, and the reflectivity of the post-taper region is a positive response to the RI. The RI sensitivity was estimated to be 382.83 dB/RIU and the thermal sensitivity is 9.893 pm/C. Cross-talk levels are modest (-1.544 103 dB/C and 568.1 pm/RIU), allowing for perfect separation of RI and thermal fluctuation.

The utilized CFBG has the following specifications: 15 nm (1562.5–1578.5 nm) bandwidth, 15 mm length, 1 nm/mm linear chirp, and reflectivity of 95 percent with > 1 dB ripples in bandwidth. An SMF was used to engrave the CFBG (single-mode fiber, SMF-28 type). Waist diameter and taper length are the key changeable parameters for taper construction, with the rotation mode turned off. The CFBG has scraped with acetone, cleaned with isopropanol, and the CFBG was placed in the laser operating area between the holders after all the parameters were established as shown in Table 1. The laser was ignited and the motors began moving at the appropriate speed

when the "taper" button was pressed with the X and Y cameras in the equipment, a point-by-point measurement of the produced taper was done as soon as the operation was completed [69].

Table 1 Parameters of shallow-tapered chirped FBG fabrication. (To use proper font size/type)

Fabrication Parameter	Value
Initial fiber diameter (μm)	125
Waist diameter (μm)	30
Left taper length (mm)	0.5
Waist taper length (mm)	5
Right taper length (mm)	0.5
Pre-heat (bit)	0
Absolute power (bit)	632
Relative power (bit)	100
Waist add (bit)	20
Pulling speed (mm/sec)	0.18

The RI sensitivity is shown in Figure 9(a), which has a good connection across the operating range. The calibration was carried out across a small range of work (8.7 * 10-3 RIU) to imitate a common use by bio-sensing, which is aided by the use of a gold layer covering the sensing region. The RI sensitivity is calculated as DI/Dn = 382.83 dB/RIU using the linear fit (R2 = 0.9822). The temperature calibration is shown in the second graph, which was done over a 50 0C period. Here the sensitivity is D/DT = 9.893 pm/C (R2 = 0.9982 which is equivalent to the 10 pm/0C for FBGs etched into fibers, the data demonstrate clear linearity, as shown in Figure 9. [40].

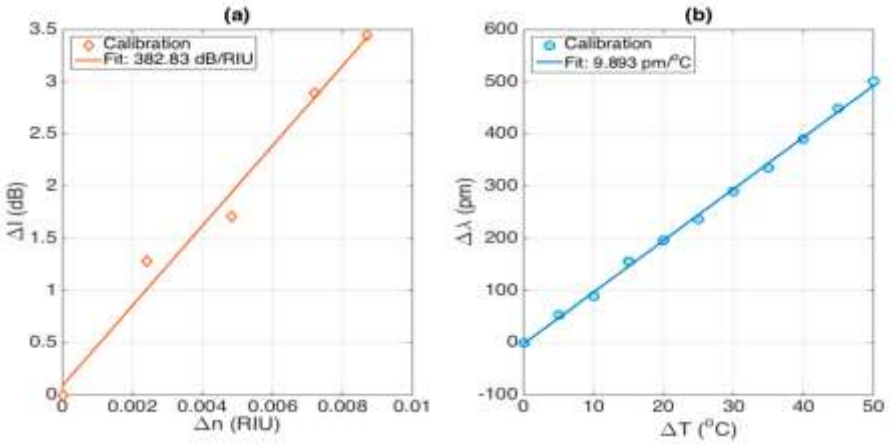

Figure 9. Sensitivity analysis results: a) RI sensitivity. b) Δλ as a function of ΔT.

The fabrication of gold-coated stCFBG to sense RI and temperature has been achieved. The fabrication is done employing a compact and shallow fiber taper with 39μm as the size of the waist and 7.29 mm length, chirped FBG. The temperature sensitivity of the pre-taper region depends on the wavelength shift, and at the same time insensitive to RI. As well as the reflectivity level is changed with the RI in the post-taper region.

O. A. Stepustchenko et al. [70] demonstrated a linearly chirped FBGs (LC-FBGs) biosensor with a refractometric fiber-optic biosensor construction and microwave photonics processing of information about the refractive index of the medium around the sensor. It is demonstrated that with a resolving power of 1.5 10–6 RIU, changes in the refractive index can be detected.

2.4 Tilted FBG Sensor

Xiaoyong Chen et al [36], proposed a tilted fiber Bragg grating (TFBG), which is a modified FBG in which the periodic planes are angled by a suitable degrees relative to the direction of propagation. The TFBG includes characteristics that allow it to detect minor changes in the RI near the surface. Some of the propagated power inside the core can escape to the cladding area due to a TFBG grating-induced breach in the cylindrical symmetry of the fiber, which can then excite hundreds of modes inside the cladding that flow backward in the cladding. The coated TFBG, also known as plasmonic TFBG, is coated with a nanofilm and has both TFBG and SPR benefits. The electromagnetic energy surrounding the metallic surface is higher than the TFBG without SPR. Higher electromagnetic energy gives more sensitivity with respect to the outer refractive index.

All materials related to the biomolecule, containing CaM (1 mM), TRP (1 mM), and buffer solutions were supported by Yukun Cui. 11-mercaptoundecanoic acid, 1-ethyl-3-(3-dimethyl-aminopropyl) carbodiimide hydrochloride (EDC), and N-hydroxysuccinimide are among the compounds. To stimulate SPR, a 50 nm thick gold nanofilm was formed on the outer surface of the TFBG, as illustrated in Figure 10. Because the fiber is cylindrical, it spun at a constant speed of 0.5 rad/s during the deposition procedure to ensure uniform dispersion of the film. When the propagation constants of the gladding modes are identical to the propagation constants of the surface Plasmon Polaritons (SPPs) modes, power coupling between these two modes areas can occur, and this phenomenon is related to the decrease in the TFBG spectrum. A small change in the RI of the metallic surface region can be measured according to the power change in the modes of the cladding in the sensing area.

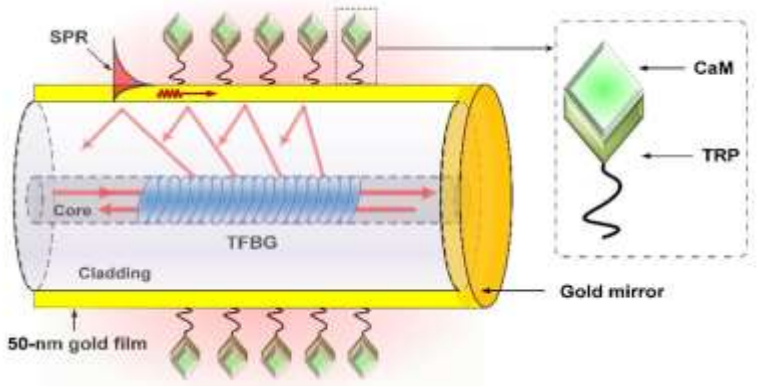

Figure 10. Detail of the proposed sensor.

For obtaining a qualitative detection, a surface functionalization process should be achieved for the plasmonic TFBG.

The TRP channels which are bounded over the metallic surface of a plasmonic TFBG in order to act as a bio-receptor were demonstrated, to detect the calmodulin. This sensor's LOD was 0.44 nM, and its operational duration was 40 minutes. Furthermore, by combining this sensor with a microfluidic device, the interaction between the CaM and TRP channels may be monitored in real-time.

Médéric Loyez et al. [72] presented a number of methods for using them in label-free immunoassays. Biofunctionalized with antibodies, bare, gold-sputtered, gold-electroless-plated (ELP), and hybrid configurations are used to detect cancer biomarkers. They explain the relative performance of the evaluated configurations and demonstrate that each leads to a unique set of critical characteristics, which drives their selection as a function of the intended application. In laboratory conditions, the sensitivity has a detection limit of 10-12 g/mL.

Maxime Lobry et al. [73] demonstrated a plasmon-assisted optical TFBG-based sensor that is non-enzymatic. For a 2 mg/mL dopamine solution, the SPR shift was around 3.83 0.05 nm after 20 minutes. Tests in several D-Glucose solutions revealed a detection limit of around 107 M, with the maximum sensitivity in the 10-6 to 10-4 M range. The limitations of conventional enzyme-based solutions can be solved with this setup.

Maxime Lobry et al. [74] investigated the relative performance of TFBGs in single-mode and multimode telecommunication-grade optical fibers for refractometry and biosensing. TFBGs are biofunctionalized using aptamers directed towards HER2 (Human Epidermal Growth Factor Receptor-2), a key protein biomarker in the detection of breast cancer. When bulk refractometry or surface biosensing are addressed, in vitro experiments demonstrate that the sensing performances of TFBGs in multimode fiber are greater or identical to those of their single-mode fiber counterparts. Numerical models corroborate these facts. TFBGs in multimode fiber provide considerable practical advantages, such as a decreased spectral bandwidth that allows for better multiplexing and detection of numerous biomarkers.

2.5 Phase Shift Fiber Bragg Grating (PSFBG)

Hardik Vyasa and Ravi Hegde [75] proposed a PSFBG that has a notch in the reflected spectrum due to a π-phase discontinuity in the center of the grating. This work proposes a PSFBG-interrogated Plasmonic nanoantenna-based intensity shift as a function of RI sensing. LSPR allows the ability to confine incident light in nanoscale volumes. They sense in ultra-low volumes of analyte (typically, modal volume V = 10−6λ3), with the detection limit can reach up to one molecule. The grating provides a Fabry Perot cavity with a high Q-factor in its turn allows more interaction of light with nanoantenna and then increases the photon lifetime. When the sensing region is surrounded by a thin layer of the analyte, the standing wave excited LSPR nanoantenna in turn causes a higher intensity variation as compared with the propagating.

Figure 11 shows the schematic of the proposed PSFBG, the phase shift is achieved by increasing the length of one of the FBG ribs. The grating sections on both sides of the cavity work as Bragg reflectors [76, 77].

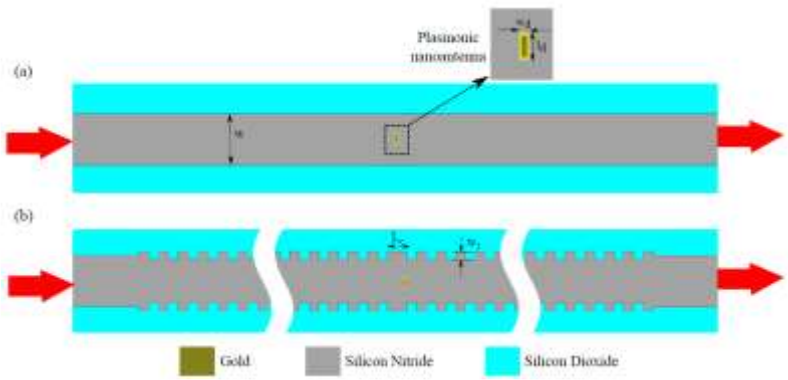

Figure 11. Schematic diagram of a plasmonic nanoantenna interrogated by (a) a strip waveguide, (b) phase shifted Bragg grating (PSBG) waveguide. The nanoantenna is positioned on the top surface of both the waveguides.

Figure 12 shows a comparison of the nanoantenna optical response loaded strip vs PSBG configurations respectively. Figure 12 (a) shows the responses of the transmission and absorption bare and nanoantenna coupled strip waveguide configurations. Figure 12(b) shows the transmission response with and without nanoantenna, they show a sharp transmission peak caused by Fabry Perot resonance inside the low transmission Bragg window. Figure 12(c) shows a 35% of light is coupled to the nanoantenna as can be observed in the figure. Figure 12(d) shows the reflected signal obtained from the input port. The amplitude of electric field disruption are shown in the Figure 12(e) & (f) respectively, which is appeared over the surfaces of both bare strip and PSBG waveguides. The Fabry Perot cavity being leaky, the field is delocalized as the standing wave modes extend into the Bragg mirrors. Figure 12(g) &(h) shows the distribution of the near-field amplitude of the nanoantenna-loaded waveguides.

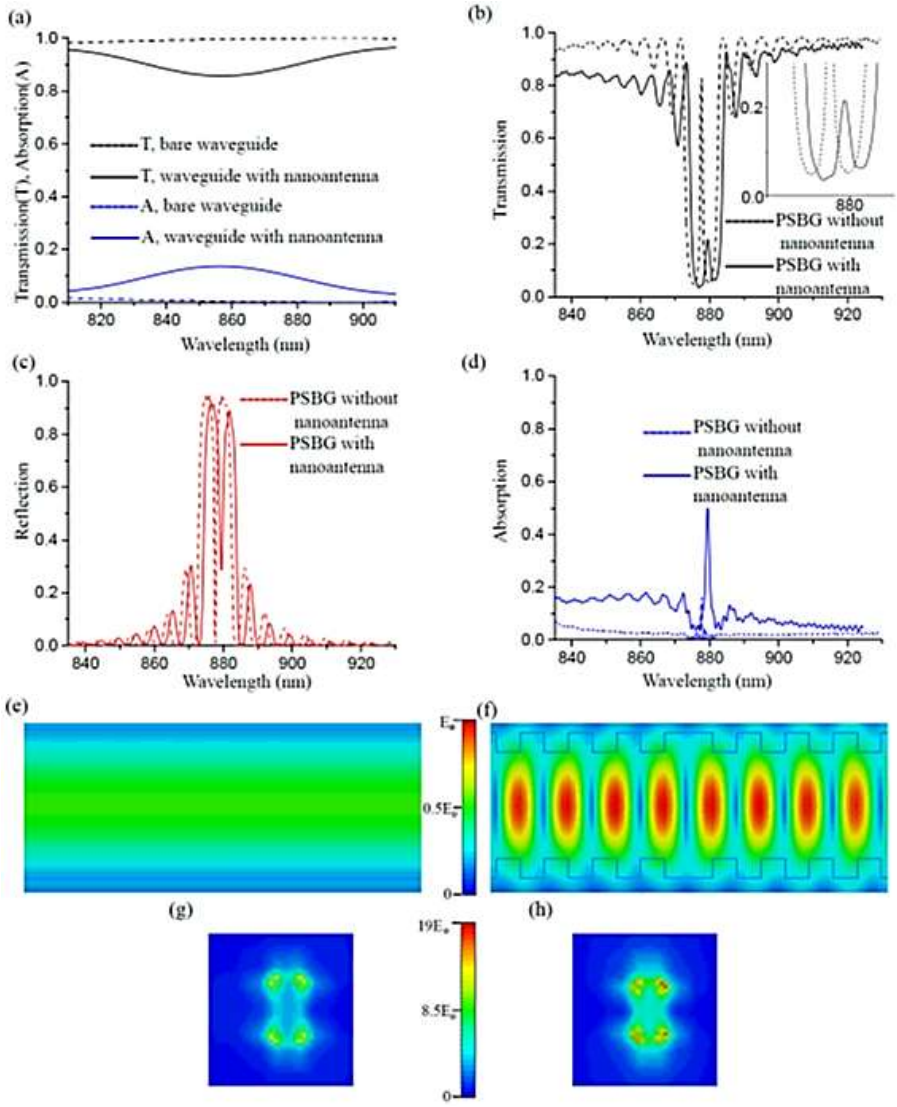

Figure 12. Comparison of the nanoantenna optical response loaded strip vs PSBG con gurations respectively.

Intensity shift due to RI variation involves monitoring the output intensity changes with a constant wavelength when the resonator (sensing element) is enclitic by the analyte. The output transmission change (dI) corresponding to the sequence value of refractive indices of analyte for both interrogation systems at a monochromatic wavelength of 879 nm is shown in the Figure 13(a). The corresponding sensitivity S is calculated as [78, 79]:

$$S = \frac{1}{I_o}\frac{dI}{dn} \tag{2}$$

Where I_o: transmission intensity in absence of analyte.

The effect of the change of geometrical parameters on the PSBG sensitivity is shown in Figure 13(a-d).

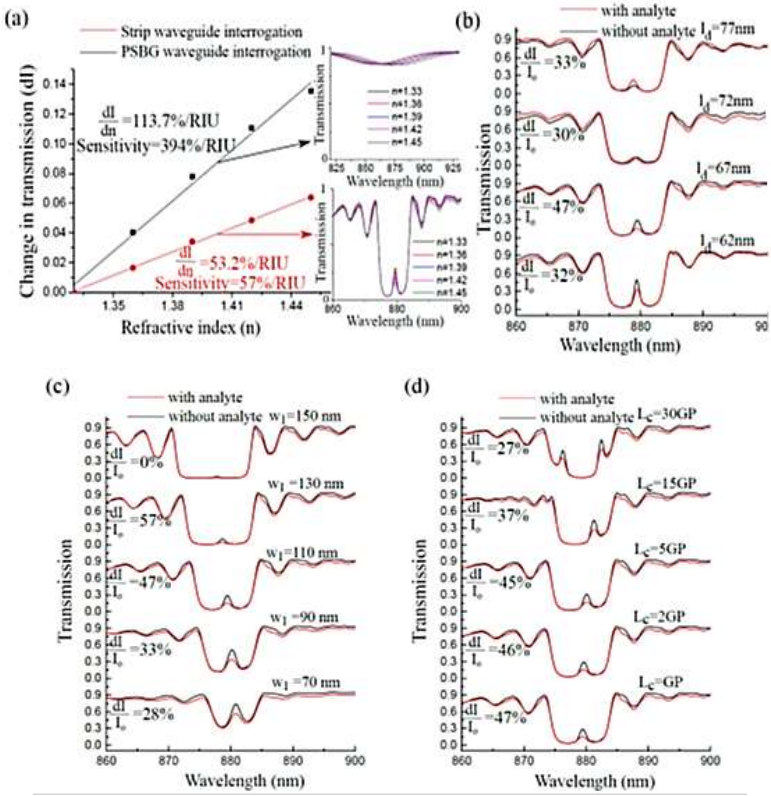

Figure 13. The performance of a plasmonic nanoantenna probed by a phase shifted Bragg grating (PSBG) waveguide in terms of intensity shift refractive index sensing. (a) Shows the transmission intensity shifts for the structure with the nanoantenna covered by a 20 nm thick analyte layer with varying refractive indices. Strip waveguide based interrogation has also been done with the same analyte. Effect of variations of geometrical parameter of PSBG waveguide system on performance of intensity sensing is shown in (b)-(d). Transmission in presence and absence of a 20nm thick analyte with refractive index 1.45 has been observed. (b) Shows the variation in transmission response for different nanoantenna lenghts (ld). The waveguide corrugation depth (w1) and cavity length (Lc) are varied in (c) and (d) respectively. The _xed geometrical parameters for the waveguide and nanoantenna have same dimensions.

A numerical study of a plasmonic nanoantenna interrogated by PSBG waveguide has been investigated for refractive index sensing application of ultra-low volumes of analytes. The interaction between the light and individual nanoantenna consequence of excitation through PSBG, is enhanced. The proposed system has been investigated based on intensity modulation using PSBG. A high sensitivity subject to changes in the grating corrugation depth and nanoantenna length has been achieved using this system.

A distributed online temperature monitoring system based on a novel hybrid FBG was proposed by Hanan M. El Gammal et al. [80]. This sensor consists of two apodized FBGs a pi-phase shift separates them. Under the variation of the variable parameters such as the grating length and the refractive index modulation amplitude, this showed an optimum remarkable performance in

terms of peak reflectivity, full width at half maximum, side lobes analysis, ripple factor, stable operation over increased temperature, and stable operation over increased temperature [81-88].

2.6 FBG in Photonic Crystal Fiber (PCF)

Olga Rusyakina et al [89], reported of extrinsic surface plasmon-enhanced refractometer based on the propagated modes inside the cladding excitation in a PCF in which the FBG is inscribed.

Six holes of air and cladding sizes of 125 and 86 μm are found in a hexagonal PCF lattice. The cross section area of PCF microstructures is imaged using a scanning electron microscope (SEM) in Fig (14). The PCFs have 8.5 mol % germanium doped in them. The diameters of air holes are about (d = 1.4 -1 μm), respectively, while the pitches are = 3.6 and 2.5 μm. For both PCFs, this results in an air-filling factor d/Λ of roughly 0.4. The diameter of the doped region with germanium is almost equal to the diameter of the air holes of both fibers. To boost photosensitivity, the PCFs were hydrogen loaded at 60°C for 60 hours under 205 bar before grating manufacture. Using ArF excimer pulsed laser with 193 nm, FBGs were inscribed onto PCFs. The gratings were created using a 250 mW average power of the laser, a 50 Hz repetition rate, and a 5 mJ laser energy pulse. The photosensitive of the first and second PCFs cores are around 1.98 kW/cm^2, and 2.8 kW/cm^2 respectively. The phase mask periods are ΛPM = 1082 nm, which inscribes FBG in the C-band with a period of ΛFBG= ΛPM/2 = 541 nm. The fiber of the proposed sensor is annealed at 70°C for 20 hours after photo-inscription. To allow spectral interrogation in transmission, the PCFs were spliced to standard SMF pigtails [90-96].

The transmission wavelength of proposed FBGs drawn in hexagonal lattice solid core PCFs with an air filling factor d/Λ = 0.4 and pitch values of 3.6 m (a) and 2.5 μm (b) are given in Fig(14) (b). Spectra are exhibited before (black) and after (dashed purple) gold deposition for the PCF indicated in (b). In this paper, the modes in the 1490-1495 nm range are employed for SPR sensing in aqueous solutions.

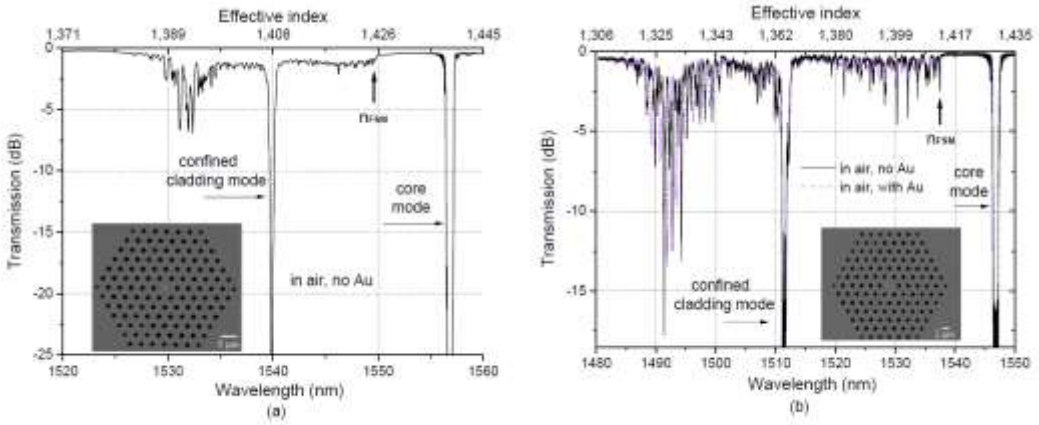

Figure 14. Straight FBGs transmission spectra inscribed in PCFs (inside hexagonal lattice).

Figure 15(a) shows the highest sensitivity of λB of about 40.3 nm/RIU and R2 = 0.9941 of the SPR-optimized polarization 1, mode 1. The largest shift of amplitude, with a (-801 dB/RIU) as a slope (R2 = 0.9937), is shown in Figure 15(b), where the wavelength of mode 2 is not linear.

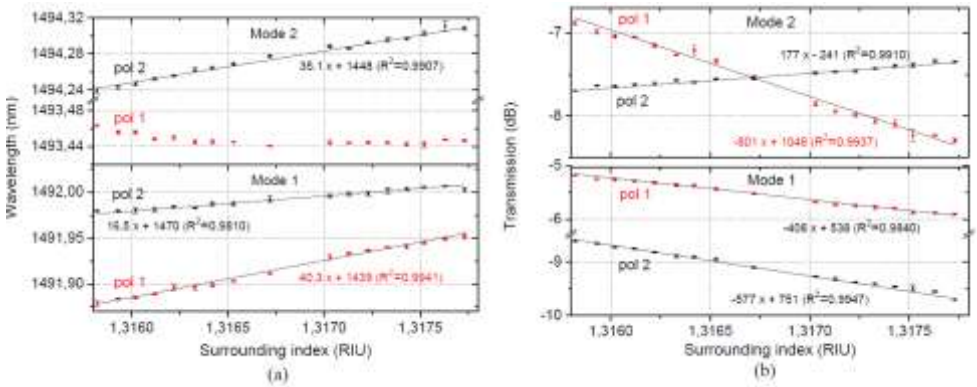

Figure 15. Highest wavelength sensitivity and the largest amplitude shift.

The inscription of straight fiber Bragg gratings is used to create this device. The gold layers have been deposited on the cladding in touch with the outer surface. The sensitivity of plasmonic to changes of the RI is in the range of (10 to 4)RIU, with the highest sensitivity of λB of about 40.3 nm/RIU and amplitude sensitivity of about -801 dB/RIU, with the linearity of more than 99%. Wavelength shifts are stable and do not have power fluctuations and are therefore often preferred. The use of multiplexed gratings in fact opens the possibility to measure different analytes/biomarkers simultaneously, in order to improve the accuracy, or for including one mode as a reference measurement.

3.0 CONCLUSION

Fiber Bragg gratings based bio-sensor represent a focus of attention of researchers; it has a unique features such as accuracy and wavelength dependence. An overview of the principles of work of many types of FBG is presented in this study. These types include tilted FBG, Uniform FBG, Chirped FBG, Long period grating, Phase-Shifted FBG, and photonics crystal FBG as a biosensor in recent years. The progress in developing these sensors for a variety of physical characteristics, including strain, force, temperature, pressure, vibration, displacement, and bio-sensors, has been evaluated. Because of its interesting advantages such as small size, high sensitivity, dynamic range, fast response, and electrical isolation, it becomes a promising field in the sensing area. Using FBG along with different types of modification in the substrate, and using a variety of physical additions, such as layers and receptors, will improve the overall sensitivity, performance, cost, and size of the sensor.

REFERENCES

[1] Alwazny, M., S., Ismail, R., A., Salim, E., T., International Journal of Nanoelectronics and Materials vol. 15 issue 3, (2022) pp. 223–232.
[2] Jitendra.K., Jitendra. S., Manoj. S., Om. P., Manoj. D., Shankar. N., IEEE Sensors Journal. vol 21 issue 6), (2021) pp. 7631-7619.
[3] AbdulAmir, H. A. A., Fakhri, M. A., Alwahib, A. A., Salim, E. T., International Journal of Nanoelectronics and Materials vol. 15 issue 2, (2022) pp. 129-138.
[4] Rui.j., Zhao, Y., Hai , H., Ji, Q., Optics & Laser Technology 125, (2020).
[5] Alwazny, M.S., Ismail, R.A., Salim, E.T., Appl. Phys. A 128, 500 (2022). https://doi.org/10.1007/s00339-022-05651-5.
[6] K.P. Nascimento, A. Frizera-Neto, C. Marques, A.G. Leal-Junior, Optical Fiber Technology vol. 65, (2021) pp. 102612.
[7] Shafeeq, S. R ., AbdulRazzaq, M. J., Salim, E. T ., Wahid, M. HA ., Key Engineering Materials, vol. 911 (2022) pp. 89-95.

[8] Markvart, A.A., Liokumovich, L.B., Medvedev, I.O., Ushakov, N.A., Journal of Lightwave Technology vol. 39 issue 1, 282-289 (2021).
[9] Jing, Y., Peng, H., Caiqian, Y., Ning, Y., Sensors. vol 21, issue 10 (2021). pp. 3492.
[10] Awayiz, M. T., Salim, E. T., AIP Conference Proceedings vol. 2213 issue 1 (2020) pp. 020247.
[11] Sridhar, S., Sebastian, S., Ajay,K., Ajay, Asokan., IEEE Sensors Journal. vol 21 issue 7 (2021) pp. 9171-9178.
[12] Juan, R., Jianfeng, Z., Xiaofeng, G., Optics Communications. Vol 488, (2021) pp. 126815.
[13] Awayiz, M. T., Salim, E. T ., Materials Science Forum vol. 1002 (2020) pp. 200-210.
[14] Toru, S., Tatsuya, I., Cryogenics . vol 113, (2021) pp. 103233.
[15] Minfu, L., Xinqiu, F., Yang, S., Shuang, L., Ningning, C., Fan, Z., Sensors . Vol 22issue7 (2022) pp. 2624.
[16] Yuanguang, Z., Bin, L., Sheng, W., Zhanbiao, Y., Applied Sciences vol 12 issue 4 (2022) p. 1781.
[17] Wanxu, Quanxi S., Heying, Q., Measurement. Vol 177, (2021) pp. 109246.
[18] Asady, H ., Salim, E. T ., Ismail, R. A., AIP Conference Proceedings vol. 2213 issue 1, (2020) p. 020183.
[19] Jianjun, D., Zhengquan, X., Gaoyang , Z., Ke. G., AIP Advances. Vol 12, issue2 (2022) pp. 025305.
[20] Xiaorong, W., Chuan, L., Zhengang, Z., Dacheng, Z., Yingna, L., Yingna, Z., Sensors.vol 21, issue15 (2021) pp.5008.
[21] Salim, E.T., Saimon, J.A., Abood, M.K., Fakhri, M.A, Optical and Quantum Electronics vol. 52issue 10 (2020) p. 463.
[22] Zamir, A., Chengyu, H., Yifan, Z., Muhammad, Q., Abdul, M., Zafarullah, A., Syed, Q., Sensors and Actuators A: Physical. Vol 331 (2021) pp. 112921.
[23] Faisal, A. D., Ismail, R. A., Khalef, W. K., Salim, E. T., Optical and Quantum Electronics vol. 52 (2020) pp. 1-12.
[24] Qinggeng, F.,a, Zhen, J., Dequan, F., Zhen, Y., Optik. Vol 225, (2021) pp. 165559.
[25] Luca, S., Juan, P., Andrea, G., Alessandro, P., Thom, B., and Luca, P., IEEE Sensors. vol 21 issue12 (2021) pp. 13263-13271.
[26] Fakhri, M.A., Khalid, F.G., Salim, E.T. Journal of Physics: Conference Series vol. 1795 issue 1 (2021) p. 012063.
[29] Fajkus, M., Nedoma, J., Martinek, R., Fridrich, M., Bednar, E., Zabka, S., Zmij, P., Sensors. Vol 21 issue15 (2021) pp.5158.
[28] Gautam, H., Asokan, S., Microelectronic Engineering. vol 248, (2021) pp. 111615.
[29] Mohsin, M.H., Numan, N.H., Salim, E.T., Fakhri, M.A., Journal of Renewable Materials vol. 9 issue 9 (2021) 1519-1530.
[30] James, A., Qimei, Z., Francisco, U., Hernandez, L., Ricardo, C., Serhiy, K., Barrie, R., Hayes, G., Ferdinand , T., Alison, P., Simon, A., and Stephen, P., Sensors. Vol 22 issue 5 (2022) pp. 1798.
[31] Bonan, L., Junxian, L., Shen, L., Yanping, C., Bo, H., Changrui, L., and Yiping, W., 2Photonic Sensors. Vol 11 issue4 (2021) pp. 411-417.
[32] Salim, E.T., Ismail, R. A. Halbos, H. T., Appl. Phys. A vol. 126, (2020) p. 891.
[33] Hongying, G., Jiang C., Zhumei, T., and Aizhen, W. Wang, Symmetry. Vol 13 issue 11 (2021) pp. 2098.
[34] Shiuh-Chuan, H., and Shin-Zhong, W. Sensors Vol 21 issue 9 (2021) pp. 3199.
[35] Ismail, R. A., Salim, E. T., Halbos, H. T., Optik, vol. 245, (2021) p. 167778.
[36] Han, Z., Xin, G., , Nan, P., Liu, J., Zhu, J., Yang, H., Optik vol. 241 (2021) 166956.
[37] Laura, F., Thomas, K., Stephen, W., Edmon, C., Alberto, V., and Ralph, P., Opt Express. Vol 29 issue 3 (2021) pp.4105-4123.
[38] Alsultany, F.H., Alhasan, S.F.H., Salim, E.T., J Inorg Organomet Polym viol. 31 (2021). Pp. 3749–3759.

[39] Manjunath, M., Uma, G., Umapathy, M., Suneetha. S., Asokan, S., Dhananjay, Y., Manjunatha A Journal of Optoelectronics and Advanced Materials. Vol 23 issue 3-4 (2021) pp. 134 - 144.
[40] Jun, W., Long, L., Shuaicheng, L., Diyang, W., Wei, W., Ming S., Guanjun W., and Mengxing, H. Photonics. Vol 8 issue 5 (2021) pp.138.
[41] Alghurabi, M. N. A. K., Mahmood, R. S., Salim, E.T., Alhasan, S.F. H., Khalid, F.G., Materials Today: Proceedings, vol. 42 (2021) pp. 2497-2501.
[42] Hareesh, K., Mankanala, N., Preeta, S. Results in Optics. Vol 2 (2021) pp.100037.
[43] Xiaoyan S., Zikun, C., Li, Z., Limu, Z., Youwang, H., Ji'an, D., Sensors and Actuators A: Physical. Vol 331, (2021) pp.112903.
[44] Alhasan, S. F. H., Bader, B.A., Salim, E.T., Materials Today: Proceedings, vol. 42, (2021) pp. 2845-2848.
[45] Ade, F., Toto, S., Wahyu, C., Bunga, M., Haryana, H., Sintechcom: Science, Technology, and Communication Journal. Vol 2 issue 1 (2021) pp.9-13.
[46] Pasquale, D., Agostino, I., and Stefania, C., IEEE Sensors Journal. Vol 21 issue 16, (2021) pp.17868-17874.
[47] Abed, A. L., Khalef, W.K., Salim, E.T., Journal of Physics: Conference Series vol. 1795 issue 1 (2021) p. 012031.
[48] Sahoo, N., Bao, W., Liu, S., Tan, Y., Zhou, K., Optical Sensors. Vol 11772, (2021) pp.1177200.
[49] Lennart, L., Julia, L., Kort, B., Bernhard, R., and Ludger. O.. IEEE Photonics Journal. vol. issue (2021) pp. 1-7.
[50] Abood, M. K., Salim, E. T., Saimon, J. A., Hadi, A. A., International Journal of Nanoelectronics and Materials vol. 14 issue 3, (2021) pp. 259-268.
[51] Kavitha B., Radhika N., Sai, S.,and Asokan, S., . IEEE Sensors Journal. vol 21 issue2 (2021) pp.1588-1595.
[52] Tawfiq, Z. H., Fakhri, M. A., Adnan, S. A., IOP Conf. Series: Materials Science and Engineering vol. 454 issue 1 (2018) p. 012173.
[53] Adnan, S. A., Tawfiq, Z. H., Fakhri, M. A., Defect and Diffusion Forum vol. 398 (2020) pp. 23-28.
[54] Ali, H. S., Fakhri, M. A., Materials Science Forum vol. 1002 (2020) pp. 282-289.
[55] Fakhri, M. A., Tawfiq, Z. H., Adnan, S. A., AIP Conference Proceedings vol. 2213 issue 1, (2020) p. 020245.
[56] Flavio, E., Lucia, S., Anubhav, S., Francesco, B., Stefania, C., Francesco, C., Michele, G., Ambra, G., Agostino, I., Biosens Bioelectron. Vol 172 (2021) pp. 112747.
[57] Fakhri, M. A ., AbdulRazzaq, M. J.., Alwahib, A. A., Muttlak, W. H., Optical Materials vol. 109 (2020) pp. 110363.
[58] Hassan, M. A., Al-Nedawe, B. M., Fakhri, M. A., Applied Optics vol. 60 issue 8, (2021) pp. 2339-2347.
[59] Mohammed, L.Z., Fakhri, M.A., Abass, A. K., Journal of Physics: Conference Series vol. 1795 issue 1 pp. 012055 (2021).
[60] Ali, H. S., Fakhri, M. A. Khalifa, Z., Journal of Physics: Conference Series vol. 1795 issue 1, (2021) pp. 012065.
[61] Hassan, N. K ., Fakhri, M. A ., Salim, E. T., Engineering and Technology Journal vol. 40 issue 2, (2022) pp. 422-427.
[62] Hassan, N. K., Fakhri, M. A., Abdulwahhab, A. W., Hashim, U., Key Engineering Materials vol. 911, (2022) pp. 65-76.
[63] Liang, L., Leonel, M., Ricardo, C., Stephen, P., Seung, L., Paddy, T., Lucy, F., Serhiy, K., Sensors and Actuators B: Chemical . vol 271(2018) pp. 24-32.
[64] Liu, C., Xu, B.J., Zhou, L., Sun, Z., Mao, H.J., Zhao, J.L., Zhang, L., Chen, X., Sensors and Actuators B: Chemical vol. 261 (2018) pp. 91-96.
[65] Flavio, E., Lucia, S., Chiara, T., Stefania, C., Michele, G., Agostino, I. Sensors and Actuators B: Chemical. Vol 274, (2018) pp. 517-526.
[66] Mandeep, S., and Sanjeev, K. Rev Sci Instrum. Vol 91 issue 12 (2020) pp.125001.

[67] Takhmina, A., Madina, S., and Daniele, T., Sensors vol 21 issue11 (2021) pp.3635.
[68] Tariq, S. M., Fakhri, M. A., Hashim, U., Key Engineering Materials, vol. 911, (2022) pp. 65-76
[69] Fakhri, M. A., Ismail, R. A., Abass, A. K., Mohammed, L. Z., Alsultany, F. H., Hashim, U., Silicon (2022). https://doi.org/10.1007/s12633-022-01902-5.
[70] Stepustchenko, O., Eshpay, R., Kurbiev, I., Proskuriakov, A., Kadushkin, V., IEEE, 2020 Systems of Signal Synchronization, Generating and Processing in Telecommunications (2020).
[71] Xiaoyong, C., Jie, J., Nan, Z., Wenwei, L., Pin. X., and Jinghua, S., Biosensors Vol 11 issue 6 (2021) pp. 195.
[72] Médéric, L., Maxime, L., Ruddy, W., and Christophe, C., Sensors vol 19 issue 11 (2019) pp.2595.
[73] Maxime, L., Driss, L., Médéric, L., Marc, D., Karima, C., Mariel, D., Christophe, C., Biosens Bioelectron. Vol 142, (2019) pp.111506 .
[74] Maxime, L., Mederic, L., Eman, M., Karima, C., Maria C., Erik, G., 4 Ruddy, W., AND Christophe, C.,. Opt Express. Vol 28 issue 5 (2020) pp.7539-7551.
[75] Vyas, H., Hegde, R., Nanophotonics and Micro/Nano Optics VoI, 11556, (2020) p. 115560C.
[76] Hassan, N. K., Fakhri, M. A., Salim, E. T., Hassan, M. A., Materials Today: Proceedings vol. 42 (2021) pp. 2769-2772.
[77] Tariq, S. M. , Fakhri, M. A., Salim, E.T., Hashim, U. , Alsultany, F.H. , Applied Optics vol. 61(issue 1 (2022) pp. 6257–6267.
[78] Amir, H. A. A. A., Fakhri, M. A., Alwahib, A. A., Salim, E. T., Alsultany, F. H., Hashim, U., Materials Science in Semiconductor Processing vol. 150 (2022) p. 106911.
[79] Amir, H. A. A. A., Fakhri, M. A., Alwahib, A. A., Salim, E. T., Alsultany, F. H., Hashim, U., Sensors and Actuators B: Chemical, vol. (2022) p. 132163.
[80] El-Sayed, H. M., A., Moustafa, M. R., H., Optical and Quantum Electronics. Vol 52(2020).
[81] Fakhri, M. A., Abdulwahhab A. W., Dawood, M. A., Raheema, A. Q., Numan, N. H., Khalid, F. G. M., Wahid, H. A., Hashim U., Salim, E. T., International Journal of Nanoelectronics and Materials vol. 11 (2018) pp.103-108.
[82] Mohsin, M.H., Ismail, R.A.,Mhadi, R.O., Appl. Phys. A vol. 127 (2021) pp. 214.
[83] Fakhri, M. A., Numan, N. H., Mohammed,Q. Q., Abdulla, M. S., Hassan,.O. S., Abduljabar, S. A., Ahmed, A. A., International Journal of Nanoelectronics and Materials vol. 11 (2018) pp. 109-114.
[84] Saimon, J. A., Mahdi, R. O., Khashan, K. S., Abdulameer, F. A., AIP Conference Proceedings vol. 2213 (2020) pp. 020312.
[85] Badr, B. A., Numan, N. H., Khalid, F. G., Fakhri, M.A., Abdulwahhab, A. W., Journal of Ovonic Research vol. 15 (2019) pp. 53-59.
[86] Mhadi, R. O., Ismail, R. A., Mohsin, M. H., Mater. Res. Express vol. 6 (2019) pp.126202.
[87] Saimon, J. A., Madhat, S. N., Khashan, K. S., Hassan, A. I., Mhadi, R.O., Nasif, R. A., AIP Conference Proceedings vol. 2045 (2018) pp. 020003.
[88] Mahdi, R. O., Hadi, A. A., Taha, J. M., Khashan, K. S., AIP Conference Proceedings vol. 2213 (2020) pp. 020309.
[89] Olga, R., Tigran, B., Karima, C., Pawel, M., Hugo, T., Christophe, C., Francis, B., and Thomas, G., Journal of Lightwave Technology vol. 40 issue 4 (2022) pp. 1121-1129. pp.
[90] Alwazny, M.S., Ismail, R.A., Salim, E.T., International Journal of Nanoelectronics and Materials, vol. 15 issue 3 (2022) pp. 223–232.
[91] Salim, E. T., Surface Review and Letters, vol. 20 issue 5 (2013) pp. 1350046.
[92] Khashan, K. S., Saimon, J. A., Hadi, A. A., Mahdi, R. O., J. Phys.: Conf. Ser. Vol. 1795 (2021) pp. 012026.
[93] Mohsin, M.H., Haider, M.J., Al-Shibaany, Z.Y.A., Haider, A. J., Mehadi, R. O., Silicon vol. 14 (2022) pp.1349–1355.
[94] Salim, E.T., Saimon, J.A., Abood, M.K., and Fakhri, M.A., Mat. Res. Express vol. 6 issue 12 (2019) pp. 126459.

[95] Hattab, F., Fakhry, M., 2012 First National Conference for Engineering Sciences (FNCES 2012) (2012) pp. 1-5.
[96] Faisal, D., Kalef, W.K., Salim, E.T., Alsultany, F.H., Journal of Ovonic Research, vol. 18 issue 2, (2022) pp. 205–212.